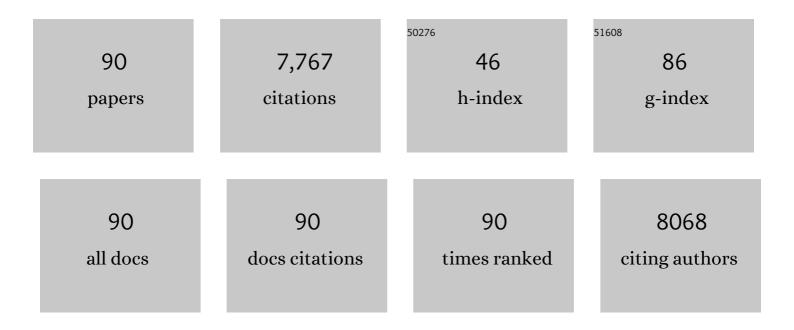
Ning Wang

List of Publications by Year in descending order

Source: https://exaly.com/author-pdf/132510/publications.pdf Version: 2024-02-01



#	Article	IF	CITATIONS
1	In Situ Confinement of Ultrasmall Pd Clusters within Nanosized Silicalite-1 Zeolite for Highly Efficient Catalysis of Hydrogen Generation. Journal of the American Chemical Society, 2016, 138, 7484-7487.	13.7	507
2	Facile Route for Synthesizing Ordered Mesoporous Ni–Ce–Al Oxide Materials and Their Catalytic Performance for Methane Dry Reforming to Hydrogen and Syngas. ACS Catalysis, 2013, 3, 1638-1651.	11.2	362
3	Carbon dots in zeolites: A new class of thermally activated delayed fluorescence materials with ultralong lifetimes. Science Advances, 2017, 3, e1603171.	10.3	286
4	Zeoliteâ€Encaged Singleâ€Atom Rhodium Catalysts: Highlyâ€Efficient Hydrogen Generation and Shapeâ€Selective Tandem Hydrogenation of Nitroarenes. Angewandte Chemie - International Edition, 2019, 58, 18570-18576.	13.8	281
5	Ultrasmall Metal Nanoparticles Confined within Crystalline Nanoporous Materials: A Fascinating Class of Nanocatalysts. Advanced Materials, 2019, 31, e1803966.	21.0	260
6	Synthesis, characterization and catalytic performances of Ce-SBA-15 supported nickel catalysts for methane dry reforming to hydrogen and syngas. International Journal of Hydrogen Energy, 2012, 37, 19-30.	7.1	245
7	Nanoporeâ€5upported Metal Nanocatalysts for Efficient Hydrogen Generation from Liquidâ€Phase Chemical Hydrogen Storage Materials. Advanced Materials, 2020, 32, e2001818.	21.0	226
8	Subnanometer Bimetallic Platinum–Zinc Clusters in Zeolites for Propane Dehydrogenation. Angewandte Chemie - International Edition, 2020, 59, 19450-19459.	13.8	221
9	Subnanometric Hybrid Pd-M(OH)2, MÂ= Ni, Co, Clusters in Zeolites as Highly Efficient Nanocatalysts for Hydrogen Generation. CheM, 2017, 3, 477-493.	11.7	212
10	A Hollow Porous CdS Photocatalyst. Advanced Materials, 2018, 30, e1804368.	21.0	204
11	A comparison study on methane dry reforming with carbon dioxide over LaNiO3 perovskite catalysts supported on mesoporous SBA-15, MCM-41 and silica carrier. Catalysis Today, 2013, 212, 98-107.	4.4	181
12	Organosilane surfactant-directed synthesis of hierarchical porous SAPO-34 catalysts with excellent MTO performance. Chemical Communications, 2014, 50, 6502.	4.1	179
13	Zeoliteâ€Encaged Pd–Mn Nanocatalysts for CO ₂ Hydrogenation and Formic Acid Dehydrogenation. Angewandte Chemie - International Edition, 2020, 59, 20183-20191.	13.8	175
14	Carbon dioxide reforming of methane for syngas production over La-promoted NiMgAl catalysts derived from hydrotalcites. Chemical Engineering Journal, 2012, 209, 623-632.	12.7	166
15	Rational design of Co9S8/CoO heterostructures with well-defined interfaces for lithium sulfur batteries: A study of synergistic adsorption-electrocatalysis function. Nano Energy, 2019, 60, 332-339.	16.0	156
16	Nâ€Đoped Graphene Modified 3D Porous Cu Current Collector toward Microscale Homogeneous Li Deposition for Li Metal Anodes. Advanced Energy Materials, 2018, 8, 1800914.	19.5	155
17	Crossâ€Coupled Macroâ€Mesoporous Carbon Network toward Record High Energyâ€Power Density Supercapacitor at 4 V. Advanced Functional Materials, 2018, 28, 1806153.	14.9	145
18	Infused-liquid-switchable porous nanofibrous membranes for multiphase liquid separation. Nature Communications, 2017, 8, 575.	12.8	143

#	Article	IF	CITATIONS
19	Synthesis, characterization and catalytic performance of MgO-coated Ni/SBA-15 catalysts for methane dry reforming to syngas and hydrogen. International Journal of Hydrogen Energy, 2013, 38, 9718-9731.	7.1	131
20	Synthesis of tri-level hierarchical SAPO-34 zeolite with intracrystalline micro–meso–macroporosity showing superior MTO performance. Journal of Materials Chemistry A, 2015, 3, 19783-19789.	10.3	121
21	High-stable α-phase NiCo double hydroxide microspheres via microwave synthesis for supercapacitor electrode materials. Chemical Engineering Journal, 2017, 316, 277-287.	12.7	118
22	Fabrication of <i>c-</i> Axis Oriented ZSM-5 Hollow Fibers Based on an in Situ Solid–Solid Transformation Mechanism. Journal of the American Chemical Society, 2013, 135, 15322-15325.	13.7	110
23	A green surfactant-assisted synthesis of hierarchical TS-1 zeolites with excellent catalytic properties for oxidative desulfurization. Chemical Communications, 2016, 52, 3368-3371.	4.1	109
24	Mesoporous nickel catalyst supported on multi-walled carbon nanotubes for carbon dioxide methanation. International Journal of Hydrogen Energy, 2016, 41, 967-975.	7.1	109
25	Manganese promoting effects on the Co–Ce–Zr–Ox nano catalysts for methane dry reforming with carbon dioxide to hydrogen and carbon monoxide. Chemical Engineering Journal, 2011, 170, 457-463.	12.7	108
26	A non-chemically selective top-down approach towards the preparation of hierarchical TS-1 zeolites with improved oxidative desulfurization catalytic performance. Chemical Communications, 2016, 52, 3580-3583.	4.1	108
27	Seeding induced nano-sized hierarchical SAPO-34 zeolites: cost-effective synthesis and superior MTO performance. Journal of Materials Chemistry A, 2016, 4, 14978-14982.	10.3	107
28	Synthesis of hierarchical TS-1 zeolites with abundant and uniform intracrystalline mesopores and their highly efficient catalytic performance for oxidation desulfurization. Journal of Materials Chemistry A, 2017, 5, 7992-7998.	10.3	100
29	Carbogenic nanodots derived from organo-templated zeolites with modulated full-color luminescence. Chemical Science, 2016, 7, 3564-3568.	7.4	99
30	High performance nanosheet-like silicoaluminophosphate molecular sieves: synthesis, 3D EDT structural analysis and MTO catalytic studies. Journal of Materials Chemistry A, 2014, 2, 17828-17839.	10.3	96
31	Preparation and characterization of a plasma treated NiMgSBA-15 catalyst for methane reforming with CO2 to produce syngas. Catalysis Science and Technology, 2013, 3, 2278.	4.1	94
32	Template-Modulated Afterglow of Carbon Dots in Zeolites: Room-Temperature Phosphorescence and Thermally Activated Delayed Fluorescence. , 2019, 1, 58-63.		92
33	A top-down approach to hierarchical SAPO-34 zeolites with improved selectivity of olefin. Microporous and Mesoporous Materials, 2016, 234, 401-408.	4.4	86
34	Ultrafast synthesis of nano-sized zeolite SAPO-34 with excellent MTO catalytic performance. Chemical Communications, 2015, 51, 16397-16400.	4.1	78
35	Bayberry-like ZnO/MFI zeolite as high performance methanol-to-aromatics catalyst. Chemical Communications, 2016, 52, 2011-2014.	4.1	77
36	Intermediate-crystallization promoted catalytic activity of titanosilicate zeolites. Journal of Materials Chemistry A, 2018, 6, 8757-8762.	10.3	77

#	Article	IF	CITATIONS
37	Centrifugation-free and high yield synthesis of nanosized H-ZSM-5 and its structure-guided aromatization of methanol to 1,2,4-trimethylbenzene. Journal of Materials Chemistry A, 2014, 2, 19797-19808.	10.3	76
38	Atmospheric pressure synthesis of nanosized ZSM-5 with enhanced catalytic performance for methanol to aromatics reaction. Catalysis Science and Technology, 2014, 4, 3840-3844.	4.1	72
39	Modulation of b-axis thickness within MFI zeolite: Correlation with variation of product diffusion and coke distribution in the methanol-to-hydrocarbons conversion. Applied Catalysis B: Environmental, 2019, 243, 721-733.	20.2	71
40	Synergetic Effect of Ultrasmall Metal Clusters and Zeolites Promoting Hydrogen Generation. Advanced Science, 2019, 6, 1802350.	11.2	70
41	Self-assembled Ni/NiO/RGO heterostructures for high-performance supercapacitors. RSC Advances, 2015, 5, 77958-77964.	3.6	67
42	In situ controllable assembly of layered-double-hydroxide-based nickel nanocatalysts for carbon dioxide reforming of methane. Catalysis Science and Technology, 2015, 5, 1588-1597.	4.1	60
43	Crystal-plane effects of MFI zeolite in catalytic conversion of methanol to hydrocarbons. Journal of Catalysis, 2018, 360, 89-96.	6.2	58
44	The recyclable synthesis of hierarchical zeolite SAPO-34 with excellent MTO catalytic performance. Chemical Communications, 2015, 51, 11987-11989.	4.1	57
45	Ni–Co bimetallic MgO-based catalysts for hydrogen production via steam reforming of acetic acid from bio-oil. International Journal of Hydrogen Energy, 2014, 39, 18688-18694.	7.1	54
46	Cost-effective synthesis of hierarchical SAPO-34 zeolites with abundant intracrystalline mesopores and excellent MTO performance. Chemical Communications, 2018, 54, 3697-3700.	4.1	54
47	Direct synthesis of c-axis oriented ZSM-5 nanoneedles from acid-treated kaolin clay. Journal of Materials Chemistry A, 2013, 1, 3272.	10.3	53
48	Improvement of catalytic stability for CO 2 reforming of methane by copper promoted Ni-based catalyst derived from layered-double hydroxides. Journal of Energy Chemistry, 2016, 25, 1078-1085.	12.9	48
49	The influence of straight pore blockage on the selectivity of methanol to aromatics in nanosized Zn/ZSM-5: an atomic Cs-corrected STEM analysis study. RSC Advances, 2016, 6, 74797-74801.	3.6	48
50	Simple Quaternary Ammonium Cations-Templated Syntheses of Extra-Large Pore Germanosilicate Zeolites. Chemistry of Materials, 2016, 28, 6455-6458.	6.7	46
51	Hydrogen Production by Ethanol Steam Reforming on NiCuMgAl Catalysts Derived from Hydrotalcite-Like Precursors. Catalysis Letters, 2011, 141, 1228-1236.	2.6	45
52	Regulation of Ni–CNT Interaction on Mn-Promoted Nickel Nanocatalysts Supported on Oxygenated CNTs for CO ₂ Selective Hydrogenation. ACS Applied Materials & Interfaces, 2018, 10, 41224-41236.	8.0	45
53	Flexible metal-templated fabrication of mesoporous onion-like carbon and Fe ₂ O ₃ @N-doped carbon foam for electrochemical energy storage. Journal of Materials Chemistry A, 2018, 6, 13012-13020.	10.3	44
54	A new ribbon-ignition method for fabricating p-CuO/n-CeO2 heterojunction with enhanced photocatalytic activity. Applied Surface Science, 2017, 403, 699-706.	6.1	43

#	Article	IF	CITATIONS
55	Spatially uniform Li deposition realized by 3D continuous duct-like graphene host for high energy density Li metal anode. Carbon, 2020, 161, 198-205.	10.3	43
56	An in-plane Co ₉ S ₈ @MoS ₂ heterostructure for the hydrogen evolution reaction in alkaline media. Nanoscale, 2019, 11, 21479-21486.	5.6	42
57	Mesoporogenâ€Free Synthesis of Hierarchical SAPOâ€34 with Low Template Consumption and Excellent Methanolâ€ŧoâ€Olefin Conversion. ChemSusChem, 2018, 11, 3812-3820.	6.8	40
58	Oneâ€pot Synthesis of Ordered Mesoporous NiCeAl Oxide Catalysts and a Study of Their Performance in Methane Dry Reforming. ChemCatChem, 2014, 6, 1470-1480.	3.7	38
59	Effects of Ce/Zr ratio on the structure and performances of Co-Ce1â^'xZrxO2 catalysts for carbon dioxide reforming of methane. Journal of Natural Gas Chemistry, 2010, 19, 117-122.	1.8	37
60	Nickel-based perovskite catalysts with iron-doping via self-combustion for hydrogen production in auto-thermal reforming of Ethanol. International Journal of Hydrogen Energy, 2012, 37, 1272-1279.	7.1	35
61	Plasma-Treated Bimetallic Ni–Pt Catalysts Derived from Hydrotalcites for the Carbon Dioxide Reforming of Methane. Catalysis Letters, 2014, 144, 293-300.	2.6	35
62	Confinement Effect of Zeolite Cavities on Methanol-to-Olefin Conversion: A Density Functional Theory Study. Journal of Physical Chemistry C, 2014, 118, 24935-24940.	3.1	32
63	In situ synthesized Li2S@porous carbon cathode for graphite/Li2S full cells using ether-based electrolyte. Electrochimica Acta, 2017, 256, 348-356.	5.2	32
64	Effect of nitrogen-containing groups on methane adsorption behaviors of carbon spheres. Journal of Analytical and Applied Pyrolysis, 2014, 107, 204-210.	5.5	30
65	A novel Ni–Mg–Al-LDHs/γ-Al2O3 Catalyst Prepared by in-situ synthesis method for CO2 reforming of CH4. Catalysis Communications, 2014, 45, 11-15.	3.3	29
66	Mesoporous MgO synthesized by a homogeneous-hydrothermal method and its catalytic performance on gas-phase acetone condensation at low temperatures. Catalysis Communications, 2016, 74, 39-42.	3.3	29
67	Pd nanoparticles immobilized on carbon nanotubes with a polyaniline coaxial coating for the Heck reaction: coating thickness as the key factor influencing the efficiency and stability of the catalyst. Catalysis Science and Technology, 2018, 8, 1423-1434.	4.1	28
68	Energy efficiency rebound effect research of China's coal industry. Energy Reports, 2021, 7, 5475-5482.	5.1	28
69	Seed-induced and additive-free synthesis of oriented nanorod-assembled meso/macroporous zeolites: toward efficient and cost-effective catalysts for the MTA reaction. Catalysis Science and Technology, 2017, 7, 5143-5153.	4.1	26
70	Remarkable carbon dioxide catalytic capture (CDCC) leading to solid-form carbon material via a new CVD integrated process (CVD-IP): An alternative route for CO2 sequestration. Journal of Energy Chemistry, 2013, 22, 136-144.	12.9	25
71	A new two-dimensional layered germanate with <i>in situ</i> embedded carbon dots for optical temperature sensing. Inorganic Chemistry Frontiers, 2018, 5, 139-144.	6.0	25
72	ReS2 nanosheets anchored on rGO as an efficient polysulfides immobilizer and electrocatalyst for Li-S batteries. Applied Surface Science, 2020, 505, 144586.	6.1	23

#	Article	IF	CITATIONS
73	Fabrication and catalytic properties of three-dimensional ordered zeolite arrays with interconnected micro-meso-macroporous structure. Journal of Materials Chemistry A, 2016, 4, 10834-10841.	10.3	22
74	Nitrogen and oxygen co-doped 3D nanoporous duct-like graphene@carbon nano-cage hybrid films for high-performance multi-style supercapacitors. Journal of Materials Chemistry A, 2017, 5, 18535-18541.	10.3	22
75	Layered perovskite-like La _{2â^'x} Ca _x NiO _{4±δ} derived catalysts for hydrogen production <i>via</i> auto-thermal reforming of acetic acid. Catalysis Science and Technology, 2018, 8, 3015-3024.	4.1	22
76	Covalently bonded 3D rebar graphene foam for ultrahigh-areal-capacity lithium-metal anodes by in-situ loose powder metallurgy synthesis. Carbon, 2020, 158, 536-544.	10.3	22
77	Molded MFI nanocrystals as a highly active catalyst in a methanol-to-aromatics process. RSC Advances, 2016, 6, 81198-81202.	3.6	21
78	Dolomite-Derived Ni-Based Catalysts with Fe Modification for Hydrogen Production via Auto-Thermal Reforming of Acetic Acid. Catalysts, 2016, 6, 85.	3.5	19
79	An estimation of regional emission intensity of coal mine methane based on coefficientâ€intensity factor methodology using China as a case study. , 2015, 5, 437-448.		18
80	Molecular insight into the enhancement of benzene-carbon nanotube interactions by surface modification for drug delivery systems (DDS). Applied Surface Science, 2017, 416, 757-765.	6.1	18
81	Rapid synthesis of rutile TiO2 nano-flowers by dealloying Cu60Ti30Y10 metallic glasses. Applied Surface Science, 2018, 428, 328-337.	6.1	16
82	Highly selective synthesis of large aromatic molecules with nano-zeolite: beyond the shape selectivity effect. RSC Advances, 2017, 7, 14309-14313.	3.6	15
83	Facile microwave-assisted synthesis of sheet-like cobalt hydroxide for energy-storage application: Effect of the cobalt precursors. Journal of Alloys and Compounds, 2015, 644, 836-845.	5.5	14
84	The role of volatiles and coal structural variation in coal methane adsorption. Science Bulletin, 2015, 60, 532-540.	9.0	12
85	Octopus-Inspired Design of Apical NiS ₂ Nanoparticles Supported on Hierarchical Carbon Composites as an Efficient Host for Lithium Sulfur Batteries with High Sulfur Loading. ACS Applied Materials & Interfaces, 2020, 12, 17528-17537.	8.0	12
86	Analyzing transfer properties of zeolites using small-world networks. Nanoscale, 2018, 10, 16431-16433.	5.6	9
87	Dealloying synthesis of SnO2TiO2 solid solution and composite nanoparticles with excellent photocatalytic activity. Applied Surface Science, 2018, 457, 200-207.	6.1	6
88	Fabrication of unique Ti0.8Sn0.2O2 double-levels nanoparticles with extremely fine structure and promising photocatalytic activity by dealloying novel Cu-Ti-Sn-Y metallic glasses. Materials Science in Semiconductor Processing, 2022, 141, 106426.	4.0	5
89	Ecological Evaluation of Industrial Parks Using a Comprehensive DEA and Inverted-DEA Model. Mathematical Problems in Engineering, 2020, 2020, 1-11.	1.1	2
90	Influence of temperature and space velocity on the MTO reaction over nano sheet-like SAPO-34 catalyst and the theoretical calculation. Scientia Sinica Chimica, 2015, 45, 383-390.	0.4	0